Efficient diagnosis of grate-fired biomass boilers by a simplified CFD-based approach

Adeline Rezeau[a*], Luis I. Díez[b], Javier Royo[b], Maryori Díaz-Ramírez[a]

[a] CIRCE, Mariano Esquillor 15, 50018-Zaragoza, Spain

[b] University of Zaragoza, María de Luna 3, 50018-Zaragoza, Spain

* Corresponding author: Adeline Rezeau, arezeau@fcirce.es

Tel. +34 976 76 29 54, Fax. +34 976 732 078

Abstract: This paper describes the development and validation of a numerical tool able to simulate biomass combustion in grate-fired systems and support operation and design improvements of these devices. The modeling method is conceived as a compromise between the demand of computing time and the degree of detail in the simulation. As such, it integrates both the bed zone and the freeboard zone on a same 3D grid and assumes the bed as a porous medium, where heterogeneous reactions are simulated by a modified laminar rate model. Liquid water, dry biomass and char are introduced as site species that react on the porous medium surfaces to produce and/or consume gas species (O_2, CO, CO_2, H_2, H_2O, light hydrocarbons and condensable gases). To validate the numerical tool, predictions have been compared to experimental data gathered in a 250 kW_{th} combustion test facility operated with a high quality woody pellet. Once validated, the tool has been applied to characterize the flow patterns as well as the temperature and the main gaseous emissions profiles within the combustion chamber. According to the analysis of the simulation results, significant improvements have been identified concerning not only operation but also design issues.

Keywords: biomass; combustion; grate firing; porous medium; Computational Fluid Dynamics (CFD)

Highlights

- A modified porous media approach was developed to simulate grate biomass combustion

- Heterogeneous reactions were modeled on the 3D porous medium surfaces
- A 250 kW_{th} boiler tested with reference woody pellets was selected as a case study
- Good validation was obtained between predictions and measured data
- Operation and design improvements were elucidated by the CFD results analysis

1 INTRODUCTION

1.1 CFD application to grate biomass combustion

Grate biomass combustion is widely applied in the European Union for heating purposes and a significant increase is expected for next decades [1]. Notwithstanding, improvements of current technologies are still needed in terms of efficiency, emissions and operation automation in order to satisfy the more and more restrictive European legislation, *e.g.*, the regulations recently published as regards energy labelling and eco-design requirements for solid fuel boilers [2, 3].

For this aim, computer-assisted tools are increasingly utilized to support the development of grate-fired technologies and numerous models have been developed for simulating solid fuels combustion in these devices, from small-scale units to large boilers. However, due to the inherent complexity in the thermo-chemical conversion of solid particles in a fuel bed, accurate modeling of all the aspects involved in grate-fired combustion is not readily achievable [4]. Depending on the main purpose of the investigation/application, a wide range of approaches and hypotheses has been considered.

In the vast majority of the works, packed bed combustion is modeled according to a two separated zones scheme: the fuel bed zone, where heterogeneous reactions occur, and the freeboard zone, where gaseous combustion takes place. The latter is usually simulated by the widely known CFD technique but, in contrast, neither conventional method is established yet nor is commercially available for modeling fuel bed combustion. Consequently, bed conversion represents the most critical stage of grate-fired combustion modeling. According to the literature, three main methods have been developed up to now: empirically derived models, stand-alone bed models and the porous medium approach. A brief review is done hereinafter.

In the first method, the inlet boundary conditions for the freeboard simulation are derived either from experimental data gathered in the vicinity of the fuel layer [5-7] or

from theoretical mass and energy balances [8, 9]. Although this method allows characterizing the main features of the gaseous combustion process in grate-fired technologies, it does not allow studying neither the effects that the primary air inlets and the porous bed have on the fluid dynamics, nor the consumption/production of chemical species due to heterogeneous reactions in the bed (*i.e.*, drying, pyrolysis and char reactions).

Concerning the stand-alone bed models, they consist in independent models developed in an external solver and coupled with the freeboard modeling by means of an exchange interface. Up to now, 1D or 2D stationary or transient bed sub-models [10-12] are the main strategies used to describe the solids combustion in a packed bed along with the discrete particle technique [13, 14] and the Euler-Euler method [15, 16]. Although this method permits to include very detailed models related to the thermo-chemical and physical processes that occur during the particle conversion, it implies a complex, long time-demanding coupling with the CFD simulation of the freeboard zone.

Finally, the porous medium approach considers the fuel bed zone as a porous volume, which includes a solid phase and a fluid phase. This zone can be integrated into the same computational domain as the freeboard zone, thus simplifying the coupling between them. The species released from heterogeneous reactions in the bed zone can be implemented in the CFD code by two main ways: as source terms, generally obtained from empirically derived data [17, 18], or by specific User-Defined Functions (UDFs), which solve the solid phase thermo-chemical conversion [19, 20].

1.2 Aims of the present study

The main purpose of our research was to develop a numerical tool able to simulate biomass combustion in grate-fired systems and support improvements of these devices. In particular, fluid patterns originated from the combustion chamber operation and design aimed to be characterized, as well as the profiles of the most relevant variables (fluid temperature and concentrations of gas species). In this sense, the simulation was required to preserve results accuracy but with reasonable development and computing demands. For these reasons, the tool was conceived according to the following specifications: 1) to model both fuel bed and freeboard zones on a unique three-dimensional grid, 2) to employ sound combustion models that adequately predict the

combustion tendencies; 3) to avoid long and critical coupling with a detailed particle-based model.

To this purpose, the porous medium approach was selected to resemble the fuel particles conversion in the packed bed. Compared to previous works applying this approach, neither sources terms nor detailed UDFs were utilized to simulate heterogeneous reactions in the bed. Instead, a modified laminar rate model was adapted in order to allow simulating drying, pyrolysis and char reactions. This enabled the integration of the reacting porous medium into a commercial CFD tool (ANSYS Fluent), together with the modeling of the freeboard section.

2 MODELING METHOD

To simulate the overall solid combustion process in 3D, the computational domain used in this work is basically composed by two fluid sub-domains: one porous fluid sub-domain that corresponds to the bed region and one simple fluid sub-domain that corresponds to the freeboard (see Fig. 1). It is worth noting that a unique fluid mixture is simulated, which flows through both the porous medium and the freeboard, and which species concentration varies in each cell according to the chemical reactions accounted for. The mixture is composed by eight gas species (O_2, CO, CO_2, H_2O, H_2, CH_4, $C_6H_{6.2}O_{0.2}$ and N_2). As concerns the solid phase, three site species (water, dry wood and char) are considered.

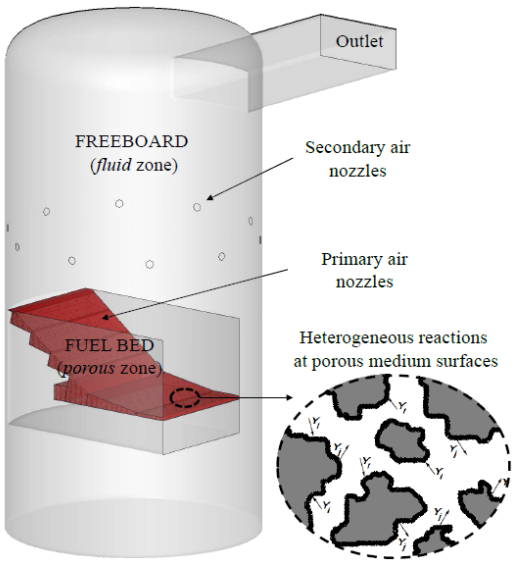

Fig. 1.- Domain with two different zones: fuel bed (porous medium) and freeboard.

2.1 Packed bed modeling

Some simplifying assumptions are adopted to carry out the modeling of the bed region:

- The porous medium sub-domain shape, size and porosity have been assumed constants during the computations, *i.e.*, stationary combustion modeling.
- The fuel bed has been considered as a unique assembly, in such a manner that individual particles movement, shrinkage or volume changes have not been simulated.
- The solid and fluid phases in the porous medium have been assumed to be at thermal equilibrium.
- Heterogeneous reactions have been assumed to occur at the porous medium surfaces and to overlap in both time and space.
- Elutriation of particles from the fuel bed has not been considered.

RANS equations of the fluid mixture have been solved in the bed zone, coupling the Ergun equation [21, 22] in the momentum conservation equation to model the resistance due to the porous medium, where the viscous and inertial factors are assumed isotropic:

$$\frac{\Delta P}{l_B} = \frac{\mu_g}{\kappa_B} v_s + C_2 \frac{\rho_g}{2} v_s^2 \qquad \text{(Eq. 1)}$$

In Eq. (1) the relation between the pressure drop $\frac{\Delta P}{l_B}$ and the velocity v_s depends on the gas thermo-physical properties μ_g and ρ_g, the bed permeability ($\kappa_B = \frac{\varphi^2 D_p^2 \epsilon_B^3}{150(1-\epsilon_B)^2}$) and the inertial factor ($C_2 = \frac{3(1-\epsilon_B)}{\varphi D_p \epsilon_B^3}$), where D_p is the equivalent spherical diameter of the particles, φ is the particle sphericity and ϵ_B is the bed porosity.

Source term of the mass conservation equation accounts for the total mass released from the surface reactions taking place in the porous medium, *i.e.*, drying, pyrolysis and char reactions. Source term of the species conservation equation ($\dot{m}_i$) includes the rate of mass (kg/m^{2}s) produced/consumed of gas species i = N_2, O_2, CO, CO_2, H_2O, H_2, CH_4, $C_6H_{6.2}O_{0.2}$ due to the N_{SR} surface chemical reactions in which gas species i participates in:

$$\dot{m}_i = M_i \sum_{r=1}^{N_{SR}} (p_{i,r} - c_{i,r}) R_r \qquad \text{(Eq. 2)}$$

Where M_i (kg/kmol) is the molecular mass of each gas species i, p and c are the stoichiometric coefficients for each gas species produced or consumed due to surface solid-gas reactions, and R (kmol/m^2 s) is the net rate of their production/consumption given by the reaction kinetics.

A reduced mechanism of five reactions has been adopted to simulate the biomass conversion in the bed region, which includes drying, devolatilization and char gasification and oxidation. Table 1 shows the set of reactions with their stoichiometry and kinetic parameters.

	#	Reaction	Arrhenius expression	Ref.
Drying	1	$H_2O_{(l)} \rightarrow H_2O$	$R_1 = 5.13 \cdot 10^{10}[H_2O_{(l)}] \exp(-88/RT)$	[26, 27]
Pyrolysis	2	Dry Wood $\rightarrow$ $0.16C_{(s)} + 0.155CO + 0.058CO_2 + 0.112H_2 + 0.043H_2O + 0.087CH_4 + 0.006C_6H_{6.2}O_{0.2}$	$R_2 = 2.62 \cdot 10^4$ [Wood] $\exp(-77.6/RT)$	[25]
Char reactions	3	$C_{(s)} + 0.5O_2 \rightarrow CO$	$R_3 = 1.4 \cdot 10^5$ $[O_2] \exp(-100.45/RT)$	[28]
	4	$C_{(s)} + CO_2 \rightarrow 2CO$	$R_4 = 6.51 \cdot 10^3 [CO_2]^{0.7} \exp(-217/RT)$	[29]
	5	$C_{(s)} + H_2O \rightarrow CO + H_2$	$R_5 = 4.45 \cdot 10^4 [H_2O]^{0.5} \exp(-217/RT)$	[29]

Table 1.- Summary of kinetic parameters used for the set of heterogeneous reactions (rates in kmol/m^{2}s; activation energies in kJ/mol; temperatures in K; concentration of site species in kmol/m^2; concentration of gas species in kmol/m^3)

Drying and pyrolysis have been assumed as single step and first order reactions and their reaction rates have been described by an Arrhenius expression. According to Ragland *et al.* [23], the non-condensable gases have been assumed to be composed primarily of CO, CO_2, H_2O, H_2 and light hydrocarbons (CH_4) and the condensable gases, or tars, have been supposed to consist of $C_6H_{6.2}O_{0.2}$. In order to assess the pyrolysis reaction stoichiometric coefficients, mass and energy balances have been calculated based on the work carried out by Thunman *et al.* [24]. The molecular mass

and the formation enthalpy of the dry wood, the volatiles, the tars and the char have also been determined according to this work, as summarized in the Appendix. Concerning char conversion, both char combustion and char gasification have been considered (see reactions 3, 4 and 5 in Table 1). Char has been assumed to consist of pure carbon and the effect of mineral matter on the conversion rates has been neglected due to the very small amount of ash in the studied fuel (as shown hereinafter).

To close the calculation of species conservation in the porous medium, it is required to set up the concentration of site species. As concerns the concentration of dry wood *[Wood]*, it is linked to the biomass flow rate, the volatiles content in the biomass, the net rate of volatiles release R_2 (see Table 1) and the bed geometry:

$$R_2 = 2.62 \cdot 10^4\ [\mathrm{Wood}] \exp(-77.6/RT) = \frac{Y_{vol} \cdot \dot{m}_F}{V_B \cdot S_B \cdot M_{vol}} \quad \text{(Eq. 3)}$$

The concentrations of the rest of site species can be related to the dry wood concentration through the biomass composition. Finally, an effective value for thermal conductivity is considered in the energy conservation equation for the bed region, accounting for both the thermal conductivity of the solid phase (bed particles) and the thermal conductivity of the gas-phase, weighted by the bed porosity:

$$\lambda_{eff} = \varepsilon_B \lambda_g + (1 - \varepsilon_B)\lambda_p \quad \text{(Eq. 4)}$$

All the thermo-physical properties of the solid phase have been estimated for a solid mix that corresponds to stationary combustion and that is constituted by dry biomass, liquid water, char and ash.

2.2 Freeboard modeling

Transport equations for the total mass of the fluid, the mass fraction of each gas species, and the conservation of momentum and energy have been also solved in the freeboard region. Available sub-models in the commercial code have been considered for simulating the turbulence closure, the heat transfer by thermal radiation and the oxidation rates of volatiles.

Correlation of velocity fluctuations have been simulated by the Realizable k- ε model [30], while thermal radiation is calculated by the P1 approach, due to its simplicity and compatibility with the finite difference modeling technique [31, 32].

Scattering is neglected and absorption coefficient is calculated by the widely known Weighted Sum of Gray Gas Model (WSGGM). This one represents a reasonable compromise between the oversimplified gray gas model and a complete model, which takes into account particular absorption bands [33]. Radiative heat contribution from the bed region has been also included in the source term of the energy conservation equation, by means of an absorption coefficient and according to the work carried out by Buczyński *et al*. [34] for fixed bed combustion in small-scale boilers.

Finite rate / Eddy dissipation model is selected to compute the release/consumption of gas species due to homogeneous oxidation of volatiles, according to the mechanism and kinetic parameters shown in the Table 2.

A summary of the modeling method developed in this work is depicted in Fig. 2.

	#	Reaction	Arrhenius expression	Ref.
Volatiles oxidation	6	$CO + 0.5O_2 \rightarrow CO_2$	$R_6 = 2.24 \cdot 10^{12}[CO][O_2]^{0.25}[H_2O]^{0.5}\exp(-167/RT)$	[35]
	7	$H_2 + 0.5O_2 \rightarrow H_2O$	$R_7 = 10^{12}[O_2][H_2]\exp(-42/RT)$	[36, 37]
	8	$CH_4 + 1.5O_2 \rightarrow CO + 2H_2O$	$R_8 = 9.2 \cdot 10^6\ T\ [CH_4]^{0.5}[O_2]\exp(-80/RT)$	[36, 37]
	9	$0.006C_6H_{6.2}O_{0.2} + 2.9O_2 \rightarrow 6CO + 3.1H_2O$	$R_9 = 1.27 \cdot 10^6\ T\ [C_6H_{6.2}O_{0.2}][O_2]\exp(-80.2/RT)$	[35]

Table 2.- Summary of kinetic parameters used for the set of homogeneous reactions (rates in kmol/m³s; activation energies in kJ/mol, temperatures in K; gases concentrations in kmol/m³)

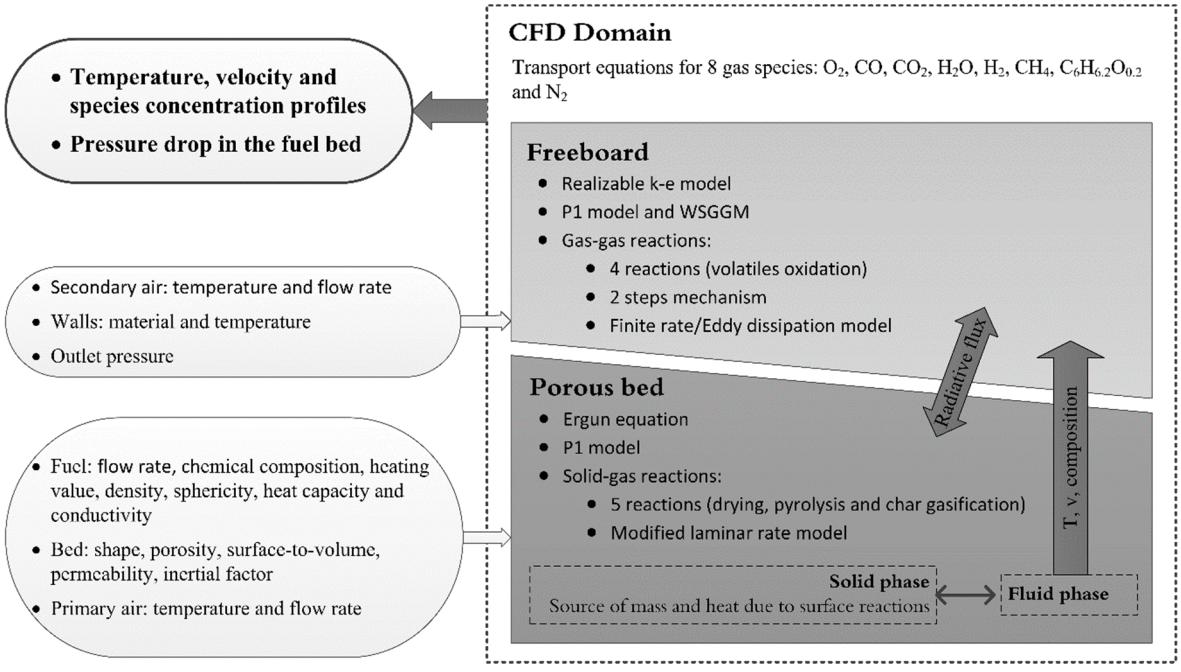

Fig. 2.- Scheme of the modeling method.

3 CASE-STUDY BOILER

3.1 Combustion test facility

The combustion test facility is a 250 kW_{th} nominal heat output boiler. This system is composed of two main devices, *i.e.*, the combustion chamber (CC from now onwards) and the heat exchanger section, which are cylindrical, constructed in carbon steel and water-cooled. A detailed scheme of the CC is shown in Fig. 3.

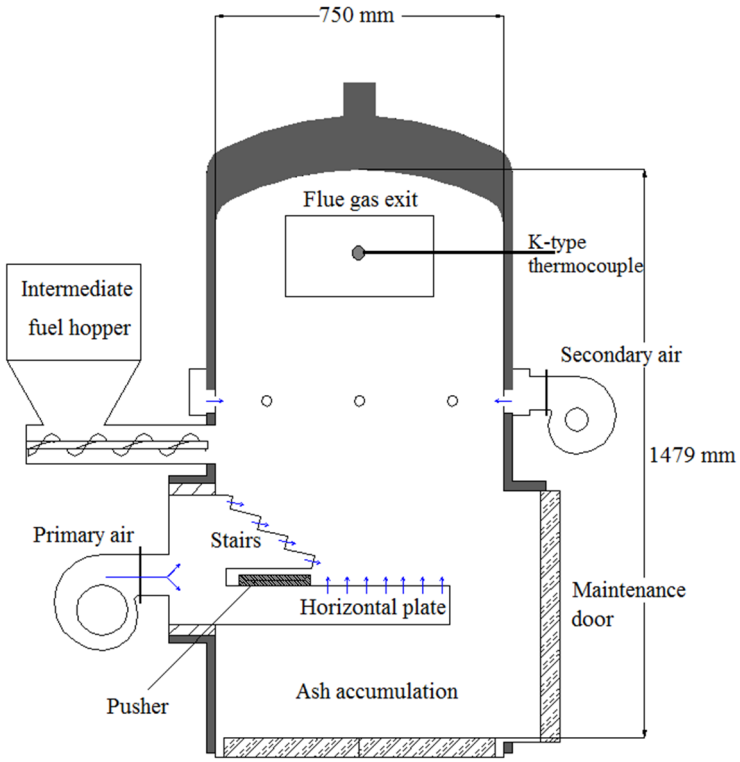

Fig.- 3. Scheme of the case-study combustion chamber.

As depicted in the Figure, the unit consists of fixed grates. They are composed by two main elements: a stair-liked grate and a horizontal plate. The fuel is continuously introduced by a screw feeder from an intermediate fuel hopper. The movement of the bed is achieved by means of gravity and the action of the fresh fuel pushing the particles already on the slightly inclined stair-like grate. After it, but before the solids fall into the bottom of the CC, the horizontal plate aims at increasing residence time and achieving a better char burnout. Moreover, a pusher is activated at a specific frequency in order to move forward the bed material and facilitate the bottom ashes removal towards the CC

bottom. For this aim, two vertical plates of refractory material are placed on both sides of the grates to avoid the burning particles to fall down before arriving at the end of the horizontal plate. With respect to the primary combustion air, it is injected under the grate (stairs + horizontal section) by means of a specific fan. Finally, the secondary air nozzles are located on a horizontal plane above the grate, *i.e.*, in the flame zone. The nozzles are uniformely distribuited in this plane, they are all oriented towards the plane center and cannot be tilted.

3.2 Fuel characterization

The selected fuel is a high quality woody pellet, produced from pine sawdust. This biofuel matches A1-class requirements of the European standard for graded wood pellets [38]. Proximate and ultimate analyses are summarized in Table 3, as well as heating values.

Proximate analysis (% wt., a.r.)		
Moisture	5.37	ISO-589
Fixed carbon	15.57	
Volatiles	78.79	ISO-5623
Ashes	0.27	ISO-1171
Ultimate analysis (% wt., d.a.f.)		
Carbon	50.72	ISO-16948
Hydrogen	5.95	ISO-16948
Sulfur	0.00	ISO-16994
Chlorine	0.00	ISO-16994
Nitrogen	0.08	ISO-16948
Oxygen	43.25	
Heating values (MJ/kg, a.r.)		
HHV	19.12	
LHV	17.77	UNE-64001

Table 3.- Biomass analysis and heating values, according to the standards.

3.3 Experimental tests

Eight experimental tests have been carried out according to a 2^3 factorial design method. The factors are the three main independent variables that could be modified during the operation of the case-study boiler: the fuel input power, $\dot{Q}_{in}$ [kW], the total excess air ratio, λ_t [-], and the primary air share, $d_{I/t}$ [%]. The latter represents the ratio

of primary air mass flow rate per total air mass flow rate injected in the combustion chamber.

For each test, data collection was performed when the steady-state regime was attained, i.e., fixed operating conditions and stable outputs. Gas concentrations of O_2, CO and NO were continuously measured in the chimney and registered every 5 seconds, thanks to a gas analyzer TESTO 350-XL. Gas temperatures were also on-line measured at the outlet of the combustion chamber and the chimney, by means of K-type thermocouples. Water flow rate in the boiler walls was continuously measured by a hydrodynamic oscillatory-type flowmeter and inlet and outlet temperatures by two PT100.

The data collected during these tests are summarized in Table 4, where the thermal efficiency of the system, calculated according to the indirect method [39], is also reported. Absolute uncertainties are also given for each variable, taking into account both systematic and random components of the total experimental uncertainty.

Threshold values from European standards can be considered as a reference to compare gaseous emissions registered during the tests. When observing Table 4, the averaged CO values are all under the limit set by the EN 303-5:2012 [39], *i.e.*, 500 mg/Nm^3 at 10 % O_2 (dry) for the strictest category (class 5). In addition, when these averaged CO emissions are compared to the Austrian deviation of EN 303-5:2012 [38, 39], the limiting values of 250 mg/MJ were satisfied in the eight tests.

With respect to NO_X emissions, no restrictions are specified by norm EN 303-5 but the results can be compared to the limit set by the Austrian deviation of this European norm. In that case, the threshold value is set to 100 mg/MJ for automatically loaded wood pellets central heaters [39, 40]. For the eight tests, averaged NO_X emissions fulfill the Austrian deviation limit.

Test	1	2	3	4	5	6	7	8
Operating conditions								
$\dot{Q}_{in}$ (kW)	200.7	200.7	200.7	200.7	268.8	239.9	260.1	239.9
λ_t (-)	1.9	2.1	1.9	2.1	1.6	1.8	1.5	1.8
$d_{I/t}$ (%)	49.8	49.1	52.8	53.7	47.6	48.5	53.1	53.4
Measured data: exhaust gas temperature and composition in dry basis								
T_G[a] (ºC)	134.0±2.4	142.3±2.4	135.3±2.4	143.8±2.4	163.0±2.4	154.8±2.4	163.3±2.5	152.4±2.5
$T_{G,CC}$[b] (ºC)	525.7±3.4	521.9±2.7	541.7±3.1	528.6±3.1	653.1±3.0	583.2±2.9	656.0±3.1	583.8±3.0
O_2 (%)	11.9±0.2	12.4±0.2	11.5±0.2	12.3±0.2	9.9±0.2	10.4±0.2	8.5±0.2	10.6±0.2
CO[c] (mg/m^3N)	193.6±11.6	215.8±12.0	175.2±10.8	208.4±11.7	446.2±29.7	103.1±10.2	273.1±19.6	105.2±10.5
CO (mg/MJ)	93.9±5.4	108.0±6.0	84.0±5.8	101.1±6.1	226.9±14.5	49.7±10.1	139.2±8.2	52.4±10.2
NO_X[d] (mg/m^3N)	143.3±12.0	167.7±12.1	142.3±12.1	175.2±12.0	134.0±12.0	172.5±12.1	123.3±12.0	164.3±12.1
NO_X[e] (mg/MJ)	68.8±3.5	80.5±4.1	68.4±3.5	84.1±4.2	68.1±3.5	83.0±10.0	61.8±3.2	79.0±10.0
Calculated data: thermal efficiency								
η_{LHV} (%)	90.13±0.25	88.90±0.29	90.41±0.24	88.91±0.29	88.97±0.26	88.92±0.24	90.01±0.23	89.95±0.24

a. Gas temperature in the chimney
b. Gas temperature at the combustion chamber outlet
c. CO concentration at 10 % O_2 (dry)
d. NO_x actual concentration at 10 % O_2 (dry) and evaluated as NO_2
e. Evaluated as NO_2

286 **Table 4. Mean values of experimental data gathered during the test, and uncertainties.**

According to current norm EN 303-5, thermal efficiency should be higher than 89 % for Class 5 boilers, which is almost satisfied in all the tested conditions (see Table 4). Nevertheless, when comparing the results to the Austrian deviation, only three tests fulfill the threshold value set at 90 % (for automatically loaded boilers with heat output comprised between 200 and 400 kW). In fact, losses due to sensible heat in the exhaust gas have been important, *i.e.*, they represent a loss comprised between 8.9 and 10.4 points on the thermal efficiency. This fact is caused by the relatively high temperature in the chimney (that could be improved by redesigning the heat exchanger section), but, and above all, by the high total excess of air that was necessary during combustion tests. In that sense, results from tests 5 and 7 show that when a lower value of total excess of air was used, combustion became unstable and CO emissions increased substantially. Accordingly, potential improvements related to minimizing total excess of air without decreasing conversion degree could be foreseen.

4 RESULTS AND DISCUSSION

4.1 CFD simulations and validation of the results

A grid constituted by 531 260 cells with one porous zone and one fluid zone has been used to model the combustion in the case-study CC. This grid has been evaluated by the method of the Grid Convergence Index, as described in a previous work [41]. This warrants the grid independence of the numerical results. Boundary conditions have been derived from experimental data depicted in Table 4 and a pressure condition of zero gauge has been assumed at the outlet section. Additionally, a non-slip condition has been considered for the solid walls, with conventional law-of-the-wall profiles for the turbulent boundary layer. In the water-cooled walls, a convective heat transfer coefficient is prescribed as a boundary condition for the simulations. This coefficient is estimated using the heat transfer rate (calculated by the available on-line measurements in the water-side) and taking into account the tubes arrangement and geometry. Concerning the solver, the pressure-based segregated algorithm has been used and the SIMPLE algorithm has been chosen for pressure-velocity coupling [42]. Finally, a second-order upwind discretization scheme has been utilized for each conservation equation.

As concerns the input parameters required to model the bed region by the porous medium approach, Table 5 shows the values used for the simulations. They have been calculated taking into account the biomass particles size and shape, and the bed geometry as well.

D_p (m)	9.97×10^{-3}
φ (-)	0.78
S_p (m^2/m^3)	766.91
ρ_p (kg/m^3)	1 734.60
ρ_{bulk} (kg/m^3)	571.90
ϵ_B (-)	0.67
S_B (m^2/m^3)	249.88
$1/\kappa_B$ (m^{-2})	849 068
C_2 (m^{-1})	475.71

Table 5.- Values for the inputs to the porous medium modeling.

The last input needed to proceed with simulations is the concentration of dry wood in the porous medium, as explained in Section 2.1. Since this is not a direct figure or estimation, an iterative procedure would be required up to get a numerical solution fulfilling Eq. (3), that is, ensuring the mass balance of the volatiles. To avoid this rather cumbersome process and aiming at designing a simplified methodology, a correlation has been obtained as a function of the three independent operating variables of the case-study unit:

$$[Wood] = -226.26 + 0.286 \cdot \dot{Q}_{in} + 33.112 \cdot \lambda_t + 4.147 \cdot d_{I/t} \quad \text{(Eq. 5)}$$

Eq. (5) was obtained after simulating iteratively three cases, and makes possible a quick calculation of the dry wood concentration to be entered to the CFD computations of the case-study facility. Comparison of the calculations *vs.* experimental data has been made according to three main parameters, as can be seen in Fig. 4: averaged O_2 and CO concentrations and gas temperature at the CC outlet. According to the comparison between calculated and measured data for all the tests, absolute differences are 5.9 %, 20.4 % and 5.8 % for O_2, CO and gas temperature, respectively.

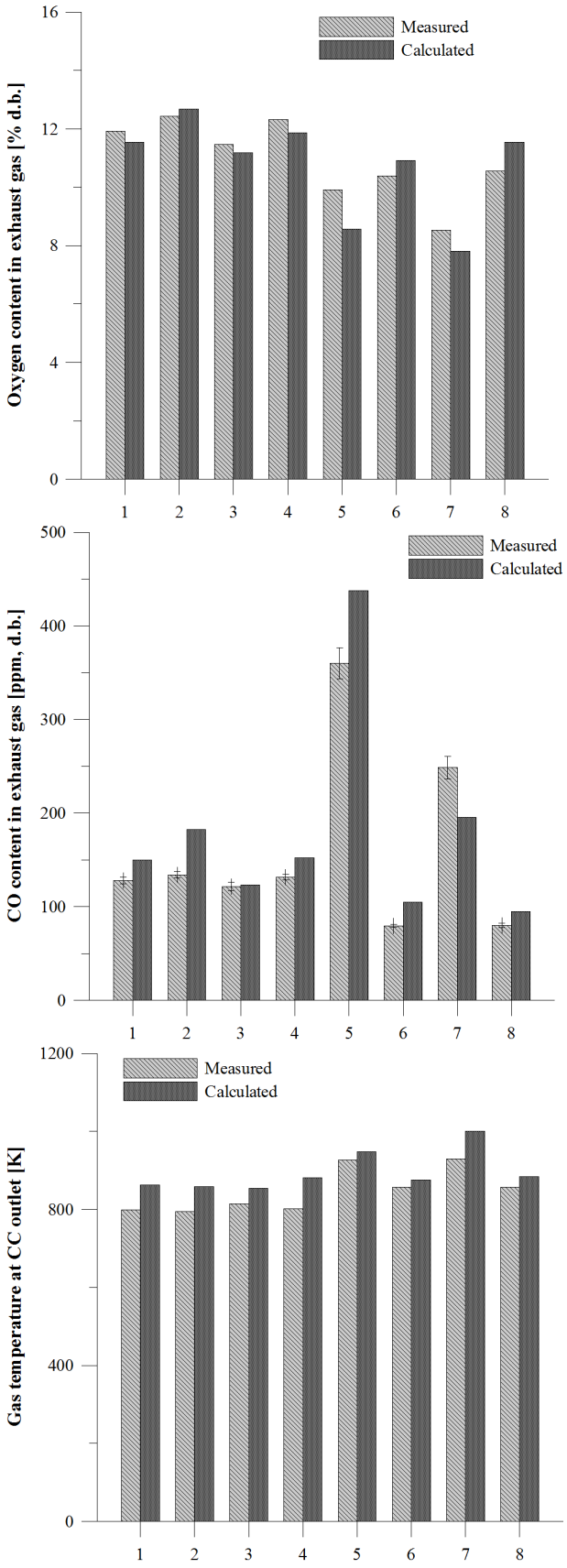

Fig. 4.- O_2 and CO concentrations and temperature at the CC outlet obtained from experimental tests and numerical simulations, tests 1 to 8.

To further study the reliability of the predicted results, linear correlation coefficients, or Pearson coefficients, have been calculated according to equations established by Hill *et al.* [43]. The coefficients obtained are respectively 0.905, 0.943 and 0.901 for O_2 content, CO content and gas temperature at the CC outlet. This indicates a strong relation and thus a good ability of the model to predict the gas temperature and its composition at the CC outlet.

Validation for CO_2 concentration is not included, since the gas analyzer did not provide that information. Nevertheless, CO_2 predictions have been found fully consistent with the carbon mass balance in the gas-phase. In consequence, the joint validation of a major species (O_2) along with a minor one (CO) can be considered accurate enough as regards the biomass conversion.

Once validated, CFD results are illustrated in Figs. 5 to 9 by means of velocity magnitude, temperature, O_2, CO and CO_2 concentrations profiles in the two planes corresponding to the middle of the CC. Streamlines are also added to stress out the flow direction and the recirculation zones obtained. These profiles correspond to tests 1, 3, 5 and 6, which are chosen for their representativeness of the overall CC behavior under different operating conditions: tests 1 and 3 correspond to a high range of O_2 concentration and a midrange of CO emissions (tests 1 to 4), test 5 to very low range of O_2 and high range of CO (tests 5 and 7) and, finally, test 6 to a midrange of O_2 and a very low range of CO (tests 6 and 8). Notwithstanding, the complete set of numerical results and illustrations may be found elsewhere [25].

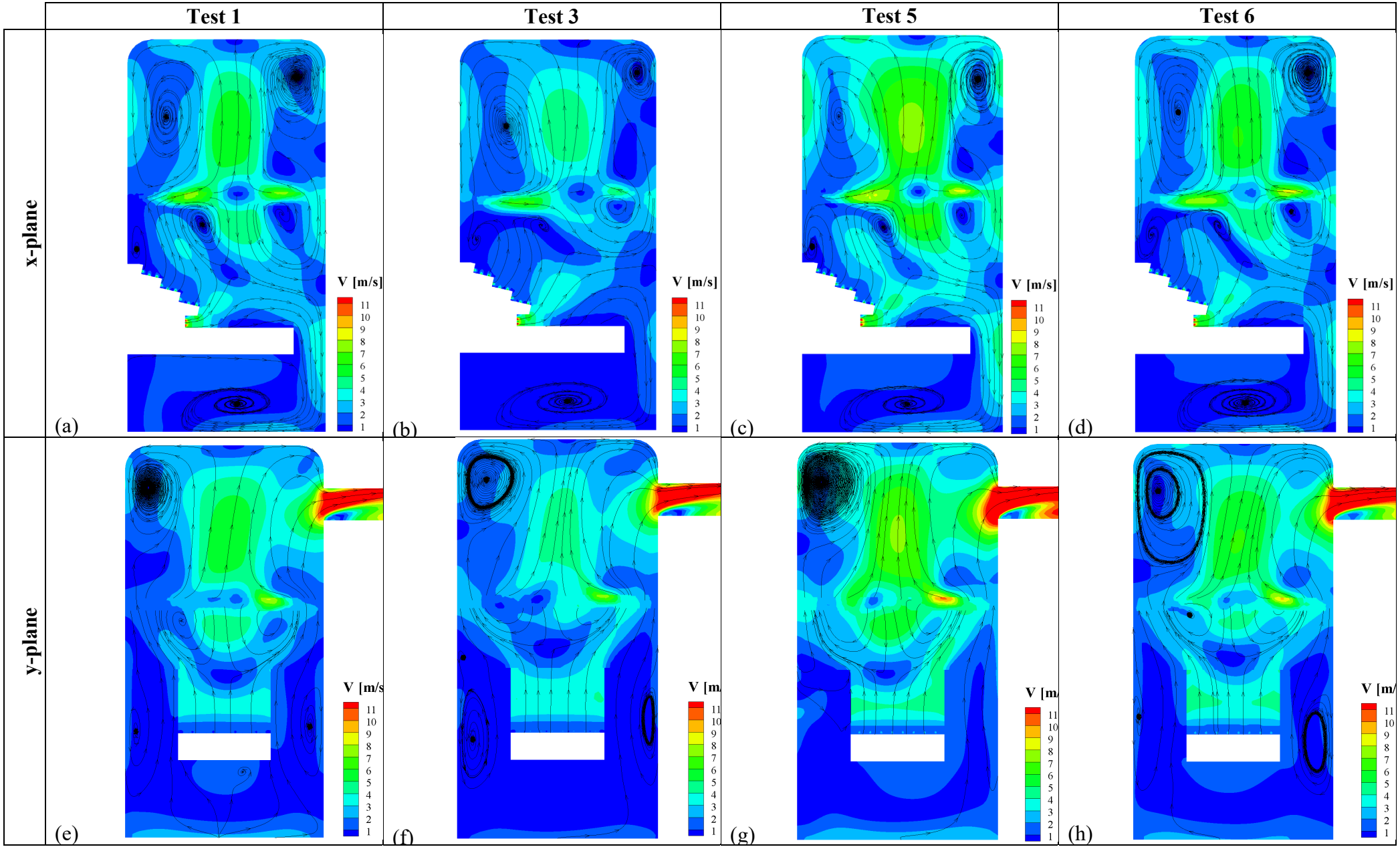

Fig 5.- Velocity profiles for tests 1, 3, 5 and 6, in x- and y-planes.

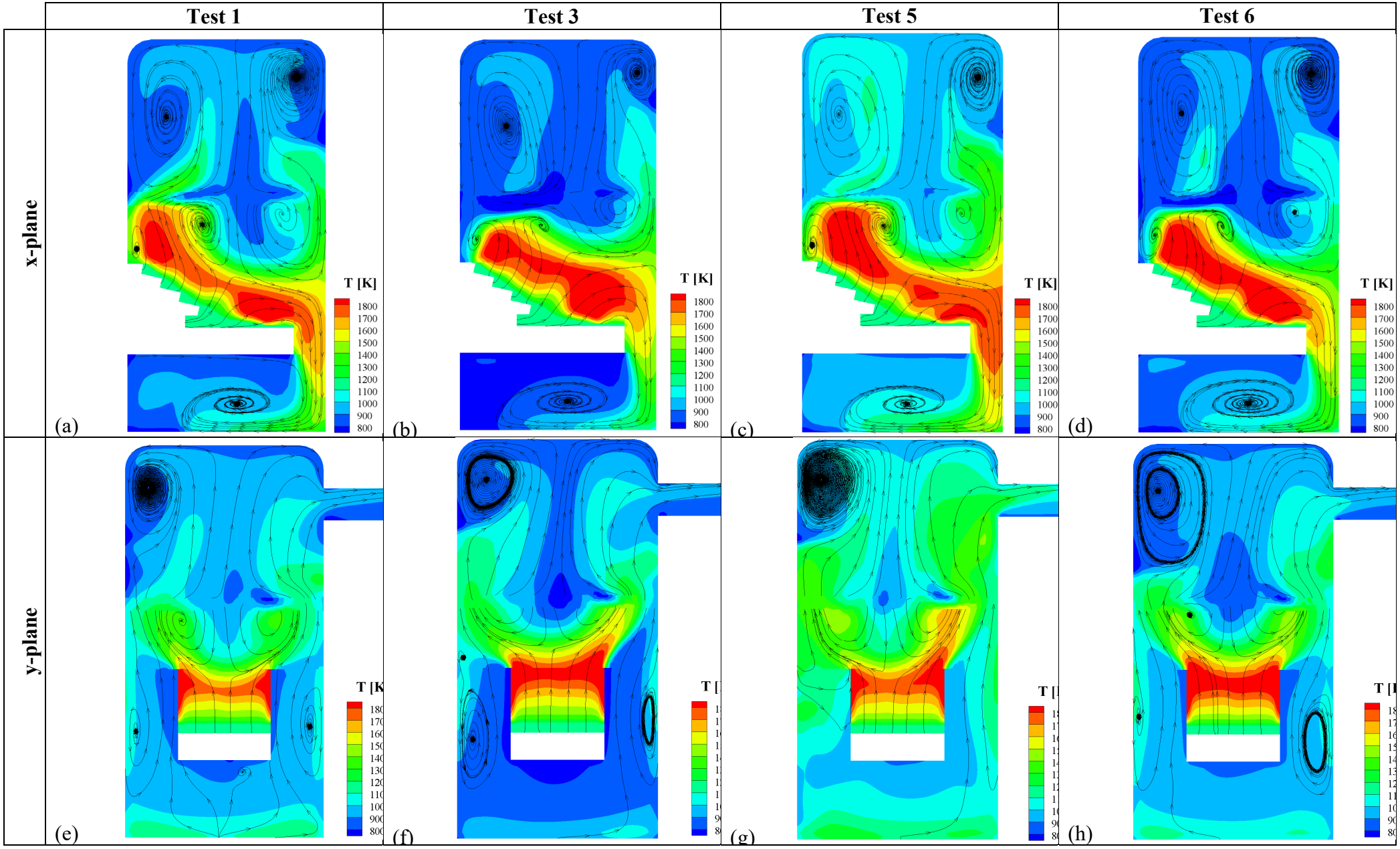

Fig. 6.- Temperature profiles for tests 1, 3, 5 and 6, in x- and y-planes.

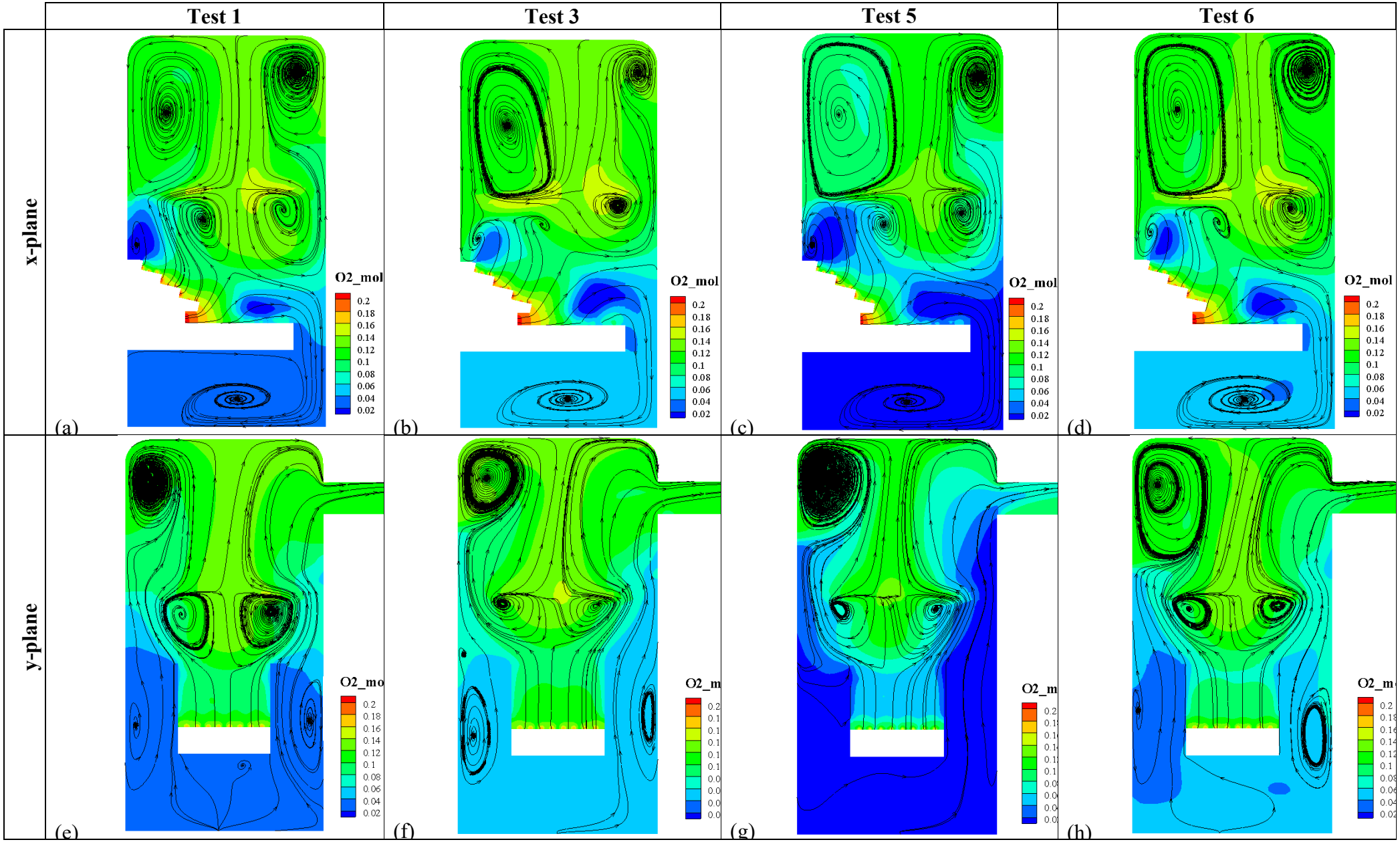

Fig. 7.- O_2 molar fraction profiles for tests 1, 3, 5 and 6, in x- and y-planes.

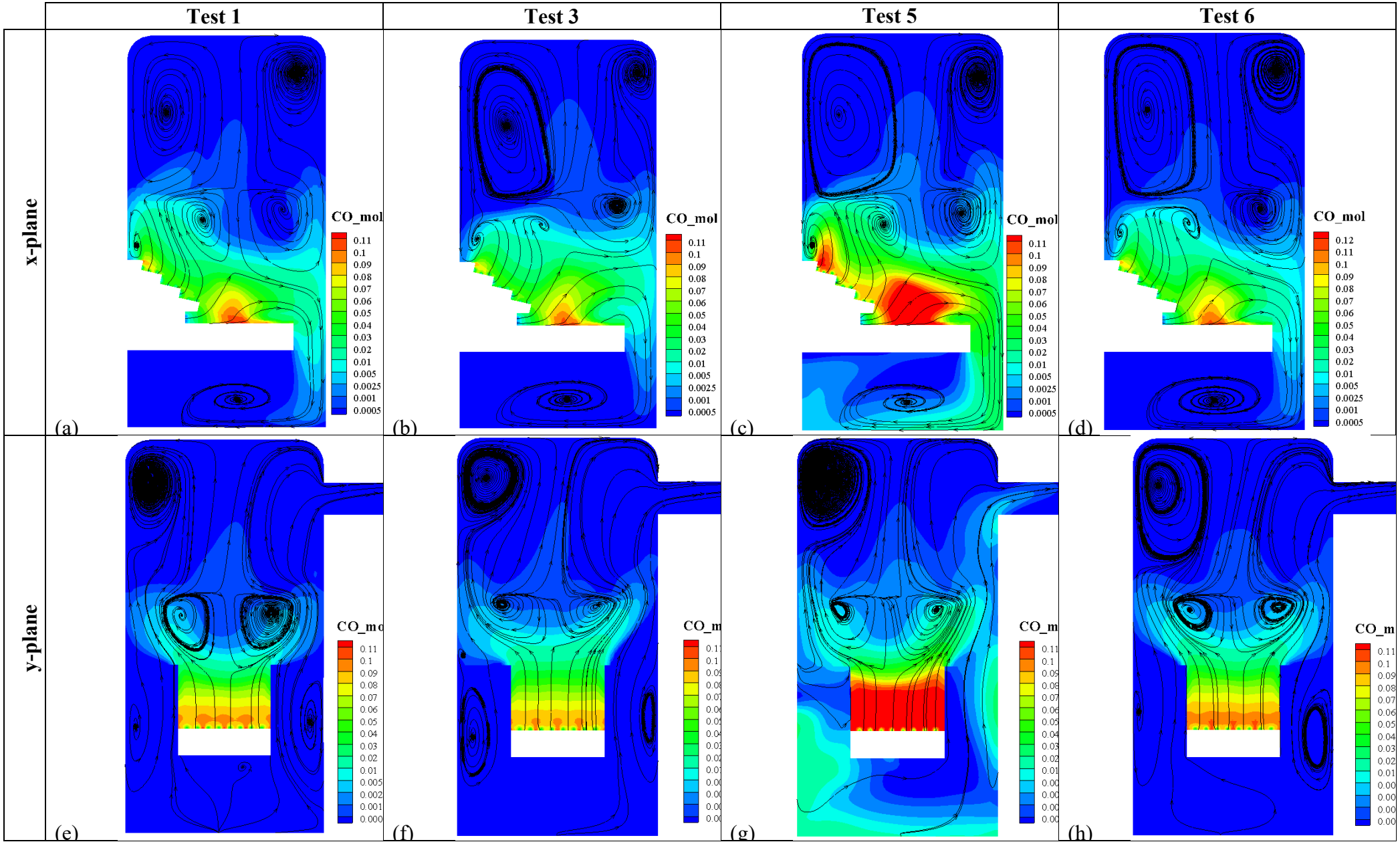

Fig. 8.- CO molar fraction profiles for tests 1, 3, 5 and 6, in x- and y-planes.

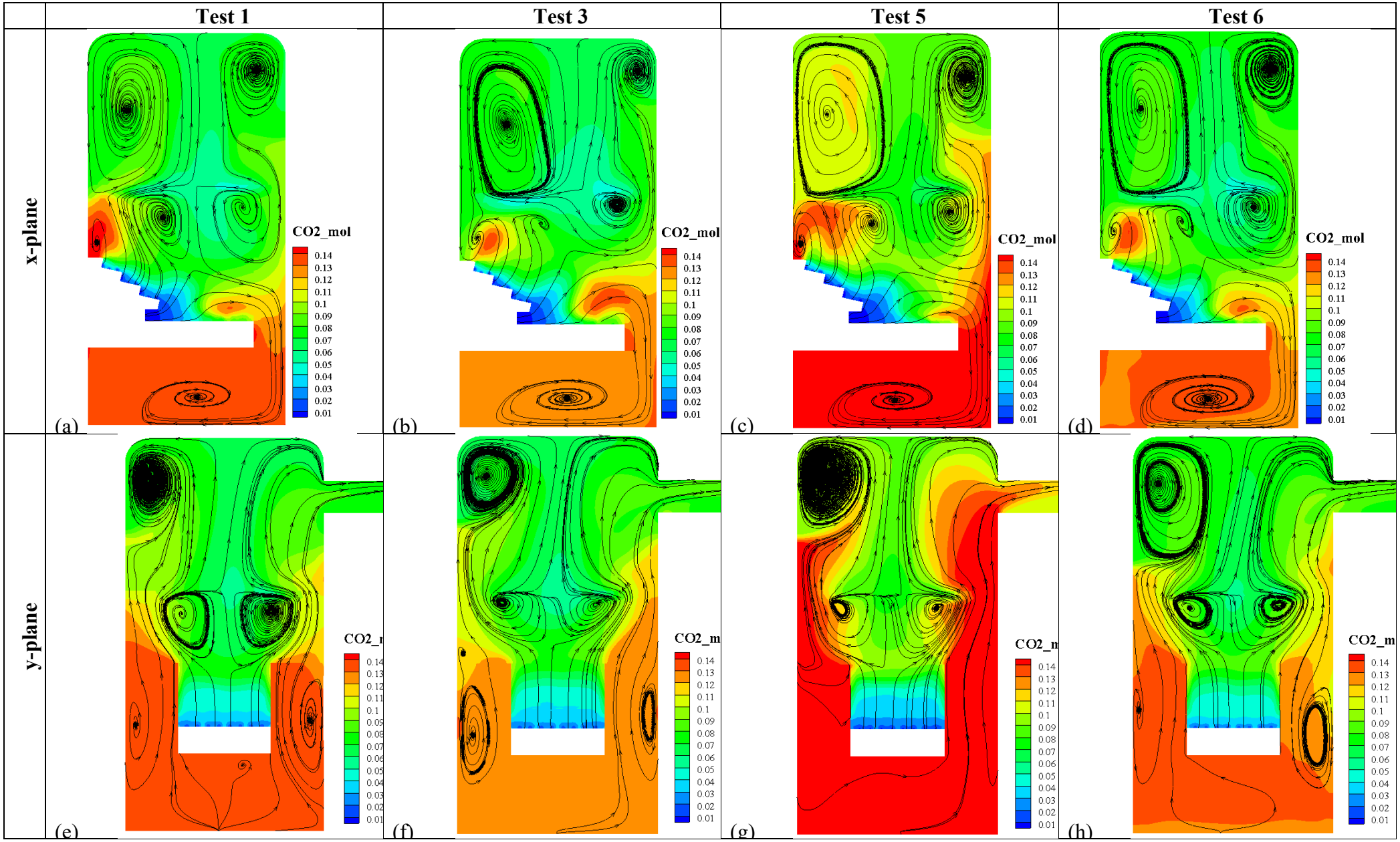

Fig. 9.- CO_2 molar fraction profiles for tests 1, 3, 5 and 6, in x- and y-planes.

4.2 Analysis of the CFD results

4.2.1 Evaluation of the tested boiler performance

According to the velocity profiles depicted in Fig. 5, it may be seen that aerodynamic features within the CC are characterized by high velocity gradients and numerous recirculation zones between the grates and the CC roof, and by a large recirculation zone in the ashtray. When focus is brought to the secondary airflow, it can be seen that high velocities appear along the axis, upwards to the CC roof but also downwards, to the horizontal plate. This peculiar phenomenon induces different facts, as described next.

Firstly, strong recirculation zones are created in the upper part when the secondary airflow does not find a direct escape, *i.e.*, upper-left and upper-right zones in x-planes (see Fig. 5.a to 5.d) and upper-left zone in y-planes (see Fig. 5.e to 5.h). As can be seen in Figs 6 to 9, these recirculation zones are characterized by relatively low temperature ($T \leq 1300$ K), high O_2 content (molar fraction > 0.1), low CO_2 content (molar fraction < 0.1) and very low CO concentration (molar fraction ≤ 0.0005). Accordingly, it may be inferred that an important fraction of the oxygen introduced by the secondary air inlets is present but almost no reactions occur with the combustion gases released from the bed, *i.e.*, a large "dead zone" appears in the upper part of the CC.

Secondly, both velocity and O_2 profiles show that part of the secondary airflow that is injected next to the exit area (Fig. 5, upper-right zone in y-planes) directly escapes to the outlet, with apparently no effective mixing. This fact is confirmed by the relatively high O_2 mass fraction calculated at the CC outlet (Fig. 7, O_2 molar fraction > 0.1).

A third aspect that arises due to the secondary air inlets configuration consists in the presence of a low temperature zone in the middle of the CC ($T \leq 1000$ K, see Fig. 6), which corresponds to the area around the intersection point where all the secondary air nozzles are oriented. This zone is characterized by very high O_2 contents (molar fractions in the range 0.12-0.14) and its area depends on the operating conditions: for tests at the same total excess of air, the higher the secondary air portion is, the wider the low temperature zone is (see Fig. 7, test 3 *vs.* test 1) and, for tests with the same air distribution, the higher the total lambda is, the wider the low temperature zone (see Fig. 7, test 5 *vs.* test 6).

Finally, it can be seen in all the tests that an important part of the secondary airflow goes downwards to the grate section where it "chocks" with the gas stream released

from the fuel bed (see Fig. 5, streamlines in both x- and y-planes). Accordingly, profiles of temperature as well as gaseous components are directly affected by this reverse or "down-flow". In particular, the flame zone, which can be defined as the area with high temperature (T ≥ 1600 K) and high CO concentrations (molar fraction > 0.04), is not located in the central zone of the CC, as it usually occurs in most of the combustion systems, but expands towards the ashtray and the CC walls (see Figs 6 and 8). As a result, high temperatures appear at the end of the horizontal plate and close to the walls, which might respectively cause ash-sintering problems when operating with low fusion temperature fuels and fatigue and deterioration of the materials. Moreover, it may be observed that this down-flow of secondary air is influenced by the air distribution. At same lambda but different primary air portion (*e.g.*, test 1 *vs.* test 3), it may be seen that the down-flow phenomenon is stronger when the primary air portion is lower. In that case, the flame zone is narrower and penetrates with higher intensity towards the ashtray.

4.2.2 Mixing characteristics within the CC

Besides the analysis of the main combustion parameters profiles, CFD results may be studied in terms of turbulence and mixing by means of the distribution of turbulent kinetic energy, k [m^2/s^2]. This parameter allows quantifying mixing phenomenon in combustion systems and was thus previously applied by some authors that studied flue gas burnout in grate biomass boilers, *e.g.*, by Zhang *et al.* [44].

In the present work, averaged and maximum k over the CFD domain have been determined for all the tests and are summarized in Table 6. In this Table, secondary air velocity at the nozzle exit (v_{II}) is also given, as well as the calculated CO concentration at the CC outlet. Moreover, the distribution of k within the CC can be observed in Fig. 10, which corresponds to test 6, *i.e.*, the one with lower concentrations of both O_2 and CO in comparison to all the other tests. As can be seen in this figure, the zone with maximum k values is located in the middle of the CC, in front of the secondary air inlets. This is also the case for the other tests, although they are not illustrated here. On the other hand, it can be observed in Table 6 that the maximum averaged value of k is 2.8 m^2/s^2 and corresponds to test 5, which has been carried out with the highest secondary air velocity at the nozzle exit. However, this test also corresponds to the highest CO emissions in the exhaust gas, as shown in Tables 4 and 6.

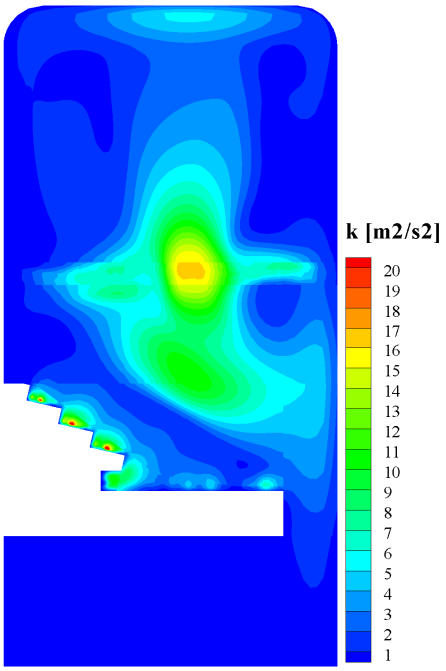

444

445 **Fig. 10.- Turbulent kinetic energy profile for test 6, in the x-plane.**

446

447

Test		1	2	3	4	5	6	7	8
v_{II}	m/s	14.9	17.2	13.9	15.7	19.2	17.4	15.0	15.7
$k_{average}$	m^2/s^2	1.7	1.9	1.4	1.7	2.8	2.1	2.0	1.7
k_{max}	m^2/s^2	49.0	63.9	64.5	82.5	82.1	86.7	81.1	88.9
CO*	mg/m^3N d.b.	218.4	301.4	172.3	229.0	483.3	143.0	203.4	137.9

448

449 **Table 6.- Turbulence parameters results for tests 1 to 8 (*: at 10 % O_2).**

450

451 In order to understand better the relation between secondary air velocity at the exit
452 and averaged k values, Fig. 11 is given. As can be observed, a linear relation is found
453 between secondary air velocity and averaged k, which confirms the fact that secondary
454 air inlets have strong impact on turbulence. Notwithstanding, if CO concentration is
455 depicted as a function of secondary air velocity, an unexpected result is obtained: CO
456 linearly increases as secondary air velocity increases, with two outliers' points for tests
457 6 and 8. According to previous authors such as Zhang *et al.* [44], reverse trend should
458 have been obtained, *i.e.*, high turbulence intensity enhances the mixing between flue gas
459 and oxygen, ensures a long combustion time and, subsequently, results in reduced

unburnt gases emissions. The result obtained in the case study CC may be explained by the fact that the zone with highest k values corresponds to the area around the intersection point where the ten secondary air nozzles are oriented. Accordingly, it can be said that the high k values registered indicate a strong mixing of the different secondary air jets among themselves, but not a mixing between secondary airflow and combustion gases.

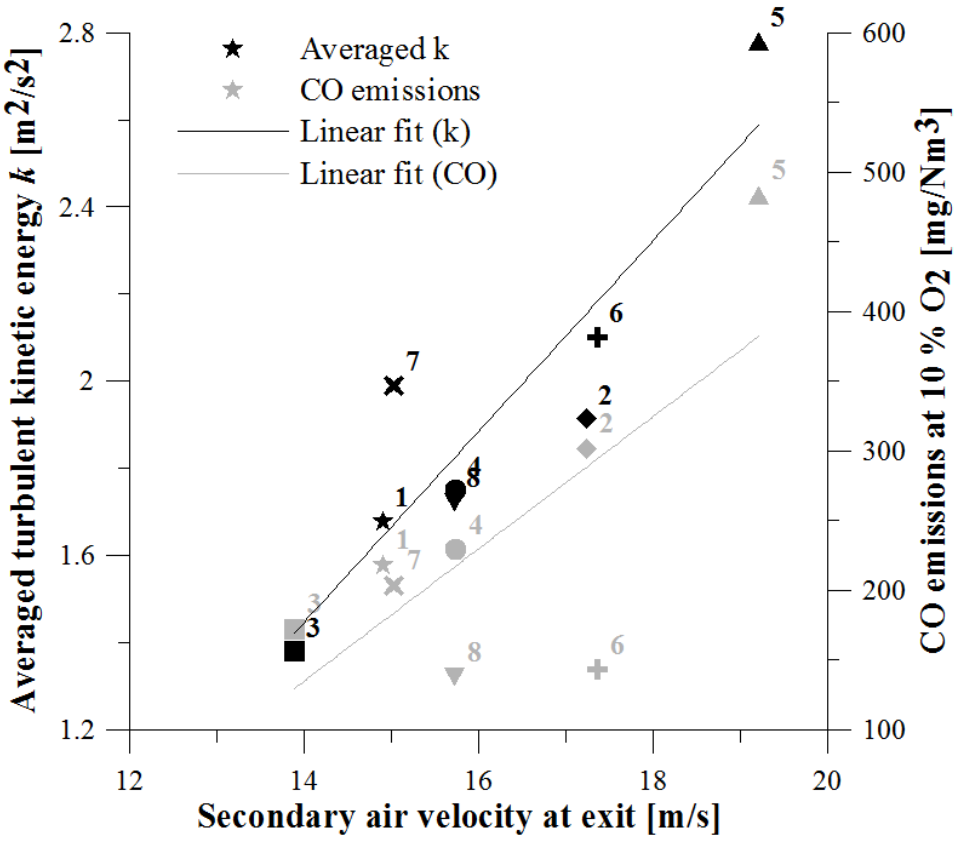

Fig. 11: Averaged k (in black) and CO emissions (in grey) as function of secondary air velocity at exit, for tests 1 to 8.

4.2.3 Global outcomes from the tested boiler and potential improvements

From the analysis of the simulation results, two main drawbacks can be inferred as regards the case-study CC design. These ones should be solved in order to improve the mixing characteristics of the device. On the one hand, the position of the grates and the "void spaces" that they leave in their surroundings create several recirculation zones and, particularly, a large dead zone in the ashtray. To minimize these effects, the ashtray volume and the lateral openings should be substantially reduced, *e.g.* by moving the

grate section at the bottom of the CC and adding a mechanical system to continuously discharge the solid residues at the end of the horizontal plate.

On the other hand, it has been seen that the secondary air inlets configuration strongly affects the aerodynamics features inside the studied CC and, consequently, the combustion process. In particular, several undesired recirculation zones are generated in the CC upper zone, as well as a strong down-flow that negatively influences the flame development. Accordingly, several modifications are induced that aim at avoiding this down-flow, creating an effective swirl in the middle of the CC, eliminating the dead zone in the upper part of the CC and reducing the overall CC volume. To do so, the secondary air nozzles location, diameter and number should be re-calculated. Firstly, nozzles should be relocated along the CC height, separating them in two or more rows and parallel-oriented (in the current configuration they are oriented towards a same point, where a high pressure zone is created). Secondly, their number and diameter should be re-adjusted to obtain a better penetration within the flue gas stream.

Finally, it is important to underline that the secondary air down-flow has also an important impact on the implementation of the air staging strategy, which aims at controlling bed temperature, fuel-NO_X emissions and ash-related problems. To do so, the recommended primary excess air ratio (*i.e.*, the ratio of excess air in the primary zone) should be comprised between 0.7 and 0.8 [45-48]. Concerning the tested device, relatively high total excess of air ($1.5 \leq \lambda_t \leq 2.1$) and high primary air portion (48.5 % $\leq d_{I/t} \leq$ 53.7 %) have been needed during the experimental tests (see Table 4). They correspond to a high primary excess air ratio, *i.e.*, between 0.77 (for test 5) and 1.13 (for test 4).

5 CONCLUSIONS

This paper has presented a new modeling approach that was developed in order to support operation and design improvements of medium-scale grate-fired biomass boilers. The method is based on the porous medium approximation and it integrates both the fuel bed zone and the freeboard on a same 3D mesh. Heterogeneous reactions are modeled on the surfaces of the porous medium, involving site and gas species and coupling an empirically derived concentration for dry wood.

Experimental tests were carried out in a 250 kW_{th} grate boiler operated with a high quality woody pellet. Good correlation coefficients were obtained between the

simulation results and the measured data, highlighting the tool capability to predict the boiler performance.

Once validated, the CFD-based tool was utilized to characterize the flow patterns within the combustion chamber, as well as the temperature and the main gaseous components profiles. Based on this analysis, several deficiencies were identified in both the operation and the design that could not have been detected with simple experimental tests. In particular, it was observed that a deficient configuration of the secondary air inlets produced several dead zones and an important down-flow, which strongly affected the combustion above the grate and forced the flame to expand towards the combustion chamber walls.

To deliver detailed guidelines and quantitatively estimate potential improvements, further research will make use of the developed tool to test the boiler under additional operating conditions and design configurations.

ACKNOWLEDGEMENTS

The research described in this paper was partially funded by the Spanish Education and Science Ministry, under the projects "On Cultivos" and 'Small-Scale Trigeneration based on Mediterranean Energy Crops and Residual Biomass Combustion". In addition, the authors would like to thank to the company LASIAN Tecnología del Calor, S.L. for allowing to use its experimental laboratory and carry out the tests that were necessary for validating the numerical model.

APPENDIX

In the present work, the pyrolysis stage has been modeled by a single-step first order reaction, as shown by Eq. A.1:

$$\text{Dry Wood} \rightarrow \gamma_{\text{char}} Char + \gamma_{volatiles} Volatiles \qquad \text{(Eq. A.1)}$$

The pyrolysis products can be distinguished as volatiles (gas phase) and carbonaceous residue or char (solid phase). The molar fractions of char and volatile matter (γ_{char} and $\gamma_{volatiles}$ respectively) have been taken from the fuel proximate analysis (see Table 3). In addition, the char has been assumed to be pure carbon.

As concerns the volatiles, they may be decomposed into condensable gases (tar) and non-condensable gases. According to Ragland et al. [23], the non-condensable gases have been assumed to be composed primarily of CO, CO_2, H_2O, H_2 and CH_4 and the condensable gases have been supposed to consist of $C_6H_{6.2}O_{0.2}$. According to these assumptions, the pyrolysis products may be written as follows, where γ_i is the molar fraction of species i in the mixture:

$$\text{Volatiles} \rightarrow \gamma_{\text{tar}}\text{Tar} + \gamma_{\text{gas}}\text{Gas} \quad \text{(Eq. A2)}$$

$$\text{Gas} \rightarrow \gamma_{\text{CO}}\text{CO} + \gamma_{\text{CO}_2}\text{CO}_2 + \gamma_{\text{H}_2}\text{H}_2 + \gamma_{\text{H}_2\text{O}}\text{H}_2\text{O} + \gamma_{\text{CH}_4}\text{CH}_4 \quad \text{(Eq. A3)}$$

In order to obtain the properties of the pyrolysis products, mass and energy balances of the pyrolysis reaction have been calculated, based on the method proposed by Thunman et al. [24].

The calculation of the molecular masses and formation enthalpies of dry wood, char, volatiles and tar requires the following information: LHV, proximate and ultimate analyses of the fuel, and molecular mass and formation enthalpy of every gas species arising in Eq. A.3. For instance, Eqs. A.4 and A.5 are used to get the formation enthalpy of dry wood:

$$\text{Dry Wood} + \gamma_{O_2} \rightarrow \gamma_{\text{CO}_2}CO_2 + \gamma_{\text{H}_2O}H_2O \quad \text{(Eq. A4)}$$

$$h^0_{wood} = \gamma_{\text{CO}_2}h^0_{CO_2} + \gamma_{\text{H}_2O}h^0_{H_2O} - \left(-LHV_{daf}\right) \cdot M_{wood} \quad \text{(Eq. A5)}$$

The same procedure can be followed for the non-condensable gases. Formation enthalpy of char is assumed to be that of pure carbon and formation enthalpy of the tar is calculated from the work by Thunman and Leckner [49]. Table 7 summarizes the results obtained for molecular masses, formation enthalpies and low heating values.

	Dry wood	Char	Gases	Tar
M (kg/kmol)	11.73	12.01	11.67	81.52
h^0 (kJ/kmol)	$-5.674\times10^{+7}$	-101.3	$-6.763\times10^{+7}$	$-9.446\times10^{+7}$
LHV (kJ/kg)	18 910	32 760	16 170	37 000

Table 7.- Properties of dry wood, char, non-condensable gases and tar.

REFERENCES

1. European Biomass Association, *AEBIOM Statistical Report 2016*.
2. *Commission Regulation (EU) 2015/1189 of 28 April 2015 implementing Directive 2009/125/EC of the European Parliament and of the Council with regard to ecodesign requirements for solid fuel boilers*.
3. *Commission Delegated Regulation (EU) 2015/1187 of 27 April 2015 supplementing Directive 2010/30/EU of the European Parliament and of the Council with regard to energy labelling of solid fuel boilers and packages of a solid fuel boiler, supplementary heaters, temperature controls and solar devices*.
4. Khodaei, H., et al., *An overview of processes and considerations in the modeling of fixed-bed biomass combustion.* Energy, 2015. **88**: p. 946-972.
5. Griselin, N. and X.S. Bai, *Emission of UHC and CO from a biomass furnace.* Progress in Thermochemical Biomass Conversion, 2001: p. 908-917.
6. Klason, T. and X.S. Bai, *Combustion process in a biomass grate fired industry furnace: a CFD study.* Progress in Computational Fluid Dynamics, 2006. **5**(4/5).
7. Buchmayr, M., et al. *A computationally inexpensive CFD approach for small-scale biomass burners equipped with enhanced air staging*. Energy Conversion and Management, 2016. **115**: p. 32-42.
8. Scharler, R., et al. *CFD analysis of air staging and flue gas recirculation in biomass grate furnaces*. in *1st World Conference on Biomass for Energy and Industry*. 2000. Sevilla, Spain.
9. Yin, C., et al., *Characterizing and modeling of an 88 MW grate-fired boiler burning wheat straw: Experience and lessons.* Energy, 2012. **41**(1): p. 473-482.
10. Ryu, C., D. Shin, and S. Choi, *Combined Simulation of Combustion and Gas Flow in a Grate-Type Incinerator.* Journal of Air & Waste Management, 2002. **52**: p. 174-185.
11. Zhang, X., et al., *Experimental investigation and mathematical modelling of wood combustion in a moving grate boiler.* Fuel Processing Technology, 2010. **91**: p. 1491-1499.
12. Porteiro, J., et al., *Numerical modeling of a biomass pellet domestic boiler.* Energy & Fuels, 2009. **23**: p. 1067-1075.
13. Peters, B., *Measurements and application of a discrete particle model (DPM) to simulate combustion of a packed bed of individual fuel particles.* Combustion and Flame, 2002. **131**(1-2): p. 132-146.
14. Wiese, J., et al., *DEM/CFD modeling of the fuel conversion in a pellet stove*. Fuel Processing Technology, 2016. **152**: p. 223-239.
15. Gómez, M.A., et al., *Eulerian CFD modeling for biomass combustion. Transient simulation of an underfeed pellet boiler.* Energy Conversion and Management, 2015. **101**: p. 666-680.
16. Le, A., et al., *System approach from biomass combustion in packed bed reactor.* Asean Journal of Chemical Engineering, 2007. **7**(1): p. 16-29.
17. Scharler, R., et al. *CFD based design and optimisation of wood log fired stoves*. in *17th European Biomass Conference and Exhibition*. 2009. Hamburg, Germany.
18. Fichet, V., et al. *A comprehensive wood combustion model for domestic stoves*. in *18th European Biomass Conference & Exhibition*. 2010. Lyon.
19. Collazo, J., et al., *Numerical modeling of the combustion of densified wood under fixed-bed conditions.* Fuel, 2012. **93**(0): p. 149-159.
20. Miltner, M., et al., *Computational fluid dynamics simulation of a solid biomass combustor: modeling approaches.* Clean Technology Envrionment policy, 2008.

21. Ergun, S., *Fluid flow through packed columns.* Chemical Engineering Progress, 1952. **48**(2).
22. Niven, R.K., *Physical insight into the Ergun and Wen & Yu equations for fluid flow in packed and fluidised beds.* Chemical Engineering Science, 2002. **57**: p. 527-534.
23. Ragland, K.W., D.J. Aerts, and A.J. Baker, *Properties of wood for combustion analysis.* Bioresource Technology, 1991. 37(2): p. 161-168.
24. Thunman, H., et al., *Composition of Volatile Gases and Thermochemical Properties of Wood for Modeling of Fixed or Fluidized Beds.* Energy & Fuels, 2001. **15**(6): p. 1488-1497.
25. Rezeau, A., *Numerical Simulation of Medium-Scale Grate-Fired Biomass Boilers*, Ph.D. Thesis, *Department of Mechanical Engineering*. 2014, University of Zaragoza.
26. Chan, W.-C.R., M. Kelbon, and B.B. Krieger, *Modeling and experimental verification of physical and chemical processes during pyrolysis of a large biomass particle.* Fuel, 1985. **64**: p. 1505-1513.
27. Bryden, K.M., K.W. Ragland, and C.J. Ruthland, *Modeling thermally thick pyrolysis of wood.* Biomass and Bioenergy, 2002. **22**: p. 41-53.
28. Senneca, O., *Kinetics of pyrolysis, combustion and gasification of three biomass fuels.* Fuel Processing Technology, 2007. **88**: p. 87-97.
29. Galgano, A. and C. Di Blasi, *Coupling a CFD code with a solid-phase combustion model.* Progress in Computational Fluid Dynamics, 2006. **6**: p. 287-302.
30. Shih, T.-H., et al., *A new k-[epsilon] eddy viscosity model for high reynolds number turbulent flows.* Computers & Fluids, 1995. **24**(3): p. 227-238.
31. Klason, T., et al., *Investigation of radiative heat transfer in fixed bed biomass furnaces.* Fuel, 2008. **87**(10-11): p. 2141-2153.
32. Liu, F., J. Swithenbank, and E.S. Garbett, *The boundary condition of the PN-approximation used to solve the radiative transfer equation.* International Journal of Heat and Mass Transfer, 1992. **35**(8): p. 2043-2052.
33. Smith, T.F., Z.F. Shen, and J.N. Friedman, *Evaluation of coefficients for the Weighted Sum of Gray Gases Model.* Journal of Heat Transfer, 1982. **104**: p. 602-608.
34. Buczyński, R., et al., *Time-Dependent Combustion of Solid Fuels in a Fixed-Bed: Measurements and Mathematical Modeling.* Energy & Fuels, 2012. **26**(8): p. 4767-4774.
35. Lu, H., *Experimental and Modeling Investigations of Biomass Particle Combustion*, Ph.D. Thesis, *Department Chemical Engineering*. 2006, Brigham Young University.
36. Di Blasi, C., *Dynamic behaviour of stratified downdraft gasifiers.* Chemical Engineering Science, 2000. **55**(15): p. 2931-2944.
37. Bryden, K.M. and K.W. Ragland, *Numerical modeling of a deep, fixed bed combustor.* Energy & Fuels, 1996. **10**: p. 269-275.
38. EN ISO 17225-2:2014, Solid Biofuels. Fuel specifications and classes. Part 2: gradded wood pellets.
39. European Committee for Standarization (CEN), *EN 303-5:2012. Heating boilers. Part 5: Heating boilers for solid fuels, manually and automatically stoked, nominal heat output of up to 500 kW. Terminology, requirements, testing and marking.* 2012.

40. *Art. 15a B-VG agreement: precautionary measures regarding small-scale heating systems with a nominal heat output up to 400 kW for residential heating*. 2011.
41. Rezeau, A., et al., *Numerical characterization of the aerodynamics in fixed-grate biomass burners.* Computers & Fluids, 2012. **69**: p. 45-53.
42. Patankar, S.V. and D.B. Spalding, *A calculation procedure for heat, mass and momentum transfer in three-dimensional parabolic flows.* International Journal of Heat and Mass Transfer, 1972. **15**(10): p. 1787-1806.
43. Hill, T. and P. Lewicki, *Statistics: methods and applications*, in *Electronic Statisstics Textbook*, I. StatSoft, Editor. 2006.
44. Zhang, J., et al. *CFD studies on the air flow in a double-grate biomass fired boiler*. in *2010 Internation Conference on Digital Manufacturing & Automation*. 2010.
45. Díaz Ramírez, M.C., et al., *Influencing factors on NO_X emission level during grate conversion of three pelletized energy crops.* Applied Energy, 2014. **115**: p. 360-373.
46. Chaney, J., et al., *An overview of CFD modelling of small-scale fixed-bed biomass pellet boilers with preliminary results from a simplified approach*, Energy Conversion and Management, 2012. **63**: p. 149-156.
47. Obernberger, I., T. Brunner, and G. Bärnthaler, *Chemical properties of solid biofuels—significance and impact.* Biomass and Bioenergy, 2006. **30**: p. 973-982.
48. Houshfar, E., et al., *NOx emission reduction by staged combustion in grate combustion of biomass fuels and fuel mixtures.* Fuel, 2012. **98**: p. 29-40.
49. Thunman, H., Leckner, B., *Thermal conductivity of wood - models for different stages of combustion*. Biomass and Bioenergy, 2002. **23**: p.47-54.

NOMENCLATURE

Acronyms

CFD	Computational Fluid Dynamics
RANS	Reynolds-Averaged Navier Stokes
WSGGM	Weighted Sum of Gray Gases Model

Roman symbols

C_2, inertial factor [m^{-1}]

$c_{i,r}$, stoichiometric coefficients for gas species i consumed by surface reaction r in the porous medium [-]

D_p, particle equivalent spherical diameter [m]

$d_{I/t}$, primary air share [%]

h^0 , formation enthalpy [kJ/kmol]

k, turbulent kinetic energy [m^2/s^2]

LHV, low heating value [kJ/kg]

$\dot{m}_F$, fuel mass flow rate in d.a.f. basis [kg/s]

$\dot{m}_i$, net rate of mass release of gas species *i* from surface reactions [kg/m^{2}s]

M_i, molecular mass of gas species i [kg/kmol]

M_{vol}, molecular mass of volatiles [kg/kmol]

M_{wood}, molecular mass of dry wood [kg/kmol]

N_b, total number of bulk species [-]

N_g, total number of gas species [-]

N_{SR}, number of surface reactions that gas species i participate in [-]

P, pressure [Pa]

$p_{i,r}$, stoichiometric coefficients for gas species i produced by surface reaction *r* in the porous medium [-]

$\dot{Q}_{in}$, fuel input power [kW]

R_r, molar rate of production/consumption of gas species by surface reaction r in the porous medium [kmol/m^{2}s]

R_{1-5}, molar rate of production/consumption of gas species by heterogeneous reactions [kmol/m^{2}s]

R_{6-9}, molar rate of production/consumption of gas species by homogeneous reactions [kmol/m^{3}s]

S_B, bed specific surface area [m^2/m^3]

S_p, particle surface-to-volume ratio [m^2/m^3]

T, temperature [K]

V_B, volume of the fuel bed [m^3]

v_S, superficial velocity in bed [m/s]

Y_{vol}, mass fraction of volatiles in fuel in d.a.f. basis [-]

Greek symbols

ϵ_B, bed porosity [-]

φ, sphericity [-]

γ, molar fraction [-]

κ_B, bed permeability [m^2]

μ_g, gas dynamic viscosity [kg/m·s]

λ_{eff}, effective thermal conductivity in the porous medium [W/m·K]

743 λ_g, gas thermal conductivity [W/m·K]

744 λ_p, thermal conductivity of the bed particles [W/m·K]

745 λ_t, total excess air ratio [-]

746 ρ_{bulk}, bulk density of the bed particles [kg/m^3]

747 ρ_g, gas density [kg/m^3]

748 ρ_p, density of the bed particles [kg/m^3]

749